

# A Class of Warm Jupiters with Mutually Inclined, Apsidally Misaligned, Close Friends

Rebekah I. Dawson,<sup>1\*</sup> Eugene Chiang<sup>1</sup>

<sup>1</sup>Department of Astronomy, University of California, Berkeley,  
501 Campbell Hall #3411, Berkeley, CA 94720-3411, USA

\*To whom correspondence should be addressed; E-mail: rdawson@berkeley.edu.

**The orbits of giant extrasolar planets often have surprisingly small semi-major axes, large eccentricities, or severe misalignments between their normals and their host stars' spin axes. In some formation scenarios invoking Kozai-Lidov oscillations, an external planetary companion drives a planet onto an orbit having these properties. The mutual inclinations for Kozai-Lidov oscillations can be large and have not been confirmed observationally. Here we deduce that observed eccentric warm Jupiters with eccentric giant companions have mutual inclinations that oscillate between 35–65°. Our inference is based on the pairs' observed apsidal separations, which cluster near 90°. The near-orthogonality of periapse directions is effected by the outer companion's quadrupolar and octupolar potentials. These systems may be undergoing a stalled version of tidal migration that produces warm Jupiters over hot Jupiters, and provide evidence for a population of multi-planet systems that are not flat and have been sculpted by Kozai-Lidov oscillations.**

Planet-planet scattering (1), secular chaos (2), and Kozai-Lidov oscillations (3, 4) induced

by a stellar (5) or planetary (6) perturber are each capable of exciting the eccentricities of giant planets (7,8), of shrinking orbits by tidal friction to form close-in hot Jupiters (having semimajor axes  $a < 0.1$  AU), and of tilting hot Jupiters' orbit normals away from their host stars' spin axes (9–14).

There are two outstanding issues with these models. First, they require or produce large inclinations between planetary orbits. These have not yet been observed. Most of the few systems with measured mutual inclinations are composed of planets on co-planar, low eccentricity, mean-motion resonant orbits, e.g., GJ 876 (15) and Kepler-30 (16). This breed of system is thought to result from gentle disk migration (17), not from Kozai oscillations, planet scattering, or secular chaos. Two notable exceptions contain well-spaced (i.e., non-resonant) giant planets. Based on astrometry with the Hubble Space Telescope fine guidance sensor, a mutual inclination of  $30^\circ$  between Upsilon Andromeda c and d was inferred (18). From transit timing variations, a mutual inclination of  $9^\circ \pm_{-6}^{+8}$  between Kepler-419 (KOI-1474) b and c was measured (19).

The second problem is that current models do not easily produce warm Jupiters, located exterior to hot Jupiters but interior to the pile-up of giant planets at 1 AU (20). Although intrinsically rare, warm Jupiters promise to distinguish among models by serving as the exception that proves the rule. Many warm Jupiters have present-day eccentricities too high to have resulted from planet-planet scattering because giant planets at small orbital distances collide and circularize before their velocity dispersions become too elevated (21). Yet most of their observed eccentricities are also too low to be easily accommodated within formation scenarios for hot Jupiters that invoke tidal migration (22), as warm Jupiters' current periapses are too far from their host stars for tidal friction to operate effectively.

One possibility (23) is that eccentric warm Jupiters are undergoing “slow Kozai” (24) migration driven by an external, mutually inclined companion. In this interpretation, warm Jupiters are observed today at the low-eccentricity phases of their secular Kozai cycles, and only rarely

attain eccentricities high enough for tidal friction to operate. For Kozai oscillations to not be quenched at these small semi-major axes by general relativistic precession, the external perturber must be nearby: it must be a “close friend” (23), in contrast to a “cold friend” (25). Supporting the possibility of migration driven by close friends, eccentric warm Jupiters orbit stars more enriched in metals — and therefore more likely to host multiple giant planets — than those of their circular counterparts (26). Indeed those warm Jupiters known to have external giant planetary companions exhibit a broader range of eccentricities than solitary warm Jupiters (23). A key question is whether the mutual orbital inclination  $i_{\text{mut}}$  between warm Jupiters and their exterior companions exceeds  $39.2^\circ$ , the minimum angle required to excite Kozai oscillations in the quadrupole approximation (3, 4). Unfortunately, nearly all these planets are detected by the radial velocity (RV) method, which does not yield  $i_{\text{mut}}$  directly, but instead measures a given planet’s  $a$ , eccentricity  $e$ , minimum mass  $m \sin i_{\text{sky}}$  (where  $i_{\text{sky}}$  is the orbital inclination with respect to the sky plane), and argument of periapse  $\omega_{\text{sky}}$  (referred to the sky plane).

However, the sky-projected apsidal separation of a planetary pair,  $\Delta\omega_{\text{sky}}$ , can be a clue to  $i_{\text{mut}}$  (27). In the invariable plane, the difference in apsidal longitudes,  $\Delta\varpi_{\text{inv}}$  (for which  $\Delta\omega_{\text{sky}}$  is our observable proxy), is often found near  $0^\circ$  or  $180^\circ$  for pairs of co-planar planets, either in the secular limit (28) or in the 2:1 mean-motion resonance (17). By contrast, for highly inclined systems, there is no such preference to find  $\Delta\varpi_{\text{inv}}$  near  $0^\circ$  or  $180^\circ$ , at least for secular systems (27). As will be shown, the behavior of  $\Delta\varpi_{\text{inv}}$  is directly reflected by its projection  $\Delta\omega_{\text{sky}}$ . Fig. 1a displays  $|\Delta\omega_{\text{sky}}|$  for RV-detected planetary pairs (29) — some of which include warm Jupiters but most of which do not — with well-constrained (30)  $e$  and  $\omega_{\text{sky}}$ , as a function of angular momentum ratio. Most systems with angular momentum ratio  $> \sim 3$  have  $|\Delta\omega_{\text{sky}}|$  near  $0^\circ$  and  $180^\circ$ . But some pairs with similarly large ratios are clustered near  $90^\circ$ .

Intriguingly, the cluster of systems having  $|\Delta\omega_{\text{sky}}| \sim 90^\circ$  includes eccentric warm Jupiters

with eccentric close friends. In fact, if we turn the problem around and consider only those systems with eccentric pairs consisting of one warm ( $0.1 < a < 1$  AU) and one “balmy” ( $a > 1$  AU) Jupiter (defined as  $m \sin i_{\text{sky}} > 0.1 M_{\text{Jupiter}}$ ) without regard for  $|\Delta\omega_{\text{sky}}|$ , then of the eight systems (31) so selected (red symbols in Fig. 1a), six (red circles) have  $|\Delta\omega_{\text{sky}}|$  near  $90^\circ$  (HD 147018, HD 38529, HD 168443, HD 74156, HD 169830, and HD 202206). The two systems we know or expect to have low mutual inclinations (red crosses) are not among these six pairs with  $|\Delta\omega_{\text{sky}}|$  clustered near  $90^\circ$ . HD 82943 (bottom red cross), is librating in the 2:1 mean motion resonance (32), which interferes with the purely secular interactions studied here by driving apsidal precession on a shorter, resonant timescale. Another outlier is the transit-detected system Kepler-419 (top red cross) which was recently found to host an eccentric pair of one warm and one balmy Jupiter having a low ( $9^\circ \pm_6^8$ ) mutual inclination and an apsidal separation of  $|\Delta\omega_{\text{sky}}| = 179^\circ.8_{-0.7}^{+0.6}$  (19). The orbital elements of all eight systems are listed in Table S1.

Here we argue that the  $\sim 90^\circ$  apsidal misalignment between warm Jupiters and their close friends signifies a mutual inclination of  $\sim 40^\circ$ , just above the lower limit for Kozai oscillations. For each of the six systems identified above (33), we perform  $\sim 1000$  numerical orbit integrations, starting with initial conditions that randomly assign the two angles not constrained by the radial-velocity data,  $i_{\text{sky}}$  and  $\Omega_{\text{sky}}$ , the latter being the longitude of ascending node on the sky plane (with the mass  $m$  chosen to satisfy the measured  $m \sin i_{\text{sky}}$ ). These angles are drawn (independently for each planet) from a uniform distribution spanning  $-1 < \cos i_{\text{sky}} < 1$  and  $0^\circ < \Omega_{\text{sky}} < 360^\circ$ , resulting in an isotropic distribution of orbits. For an additional 180 simulations, we fix  $i_{\text{sky},1} = i_{\text{sky},2} = 90^\circ$  and  $\Omega_{\text{sky},2} = 0^\circ$ , and draw  $\Omega_{\text{sky},1}$  from a uniform distribution spanning  $0^\circ$  to  $180^\circ$ . The eccentricities, semi-major axes, mean anomalies, and  $\omega_{\text{sky}}$ ’s are set to those observed. All numerical integrations in this paper use the  $N$ -body code Mercury6 (34) with the Bulirsch-Stoer integrator (bs), modified to include general-relativistic precession (35).

In Fig. 1b, we plot the fraction of time each simulated stable system spends having  $75^\circ < |\Delta\omega_{\text{sky}}| < 135^\circ$ , as a function of median mutual inclination, for five of our six systems (the sixth is a special case discussed below). Note that  $\Delta\omega_{\text{sky}} = 270^\circ = -90^\circ$  is equivalent to  $90^\circ$  in that both yield  $|\Delta\omega_{\text{sky}}| = 90^\circ$ . Each simulation is inspected by eye to ensure that the integration duration is long enough to sample the behavior of  $\Delta\omega_{\text{sky}}$ ; integration durations range from 0.15 to 100 Myr. A similar exploration of parameter space (36) was performed for two of our systems, HD 38529 and HD 168443, but without our aim of identifying regions of parameter space where  $|\Delta\omega_{\text{sky}}|$  lingers near  $90^\circ$ . As illustrated in Fig. 1b, in the five systems, we encounter configurations in which  $|\Delta\omega_{\text{sky}}|$  spends excess time near  $90^\circ$  — but only for median  $i_{\text{mut}} \sim 39^\circ$ , near Kozai’s critical inclination. For such systems,  $|\Delta\omega_{\text{sky}}|$  spends  $1/2 - 2/3$  of the time between  $75^\circ$  and  $135^\circ$ , depending on initial conditions. By comparison, uniform circulation of  $|\Delta\omega_{\text{sky}}|$  gives a fractional time of  $1/3$ . Nearly co-planar systems for which  $|\Delta\omega_{\text{sky}}|$  librates about  $0^\circ$  or  $180^\circ$  may spend no time at all in the desired range. Such realizations are inconsistent with the radial-velocity data and accordingly do not appear in Fig. 1b. The sixth system, HD 202206, is distinctive because its warm Jupiter is much more massive than the outer companion and because it lies near the 5:1 resonance. For this system, we still encounter configurations with  $i_{\text{mut}} \sim 40^\circ$  spend that excess time with  $|\Delta\omega_{\text{sky}}|$  near  $90^\circ$ , but not in the conventional range of  $75-135^\circ$ . An example shown in Fig. S5.

We reiterate that those integrations exhibiting libration of  $|\Delta\omega_{\text{sky}}|$  about  $90^\circ$  all have  $i_{\text{mut}}$  close to  $39.2^\circ$ ; typically  $i_{\text{mut}}$  varies within an interval that does not fall outside  $35-65^\circ$  over the course of a given integration. In contrast, nearly co-planar, polar, or retrograde configurations consistent with the radial-velocity data have  $|\Delta\omega_{\text{sky}}|$  circulating in the integrations we performed. Fig. 2 shows examples of how the apsidal separation lingers near  $90^\circ$  and  $270^\circ$ , in the sky plane and invariable plane, over many secular oscillations. The desired libration of  $|\Delta\omega_{\text{sky}}|$  does not require a finely-tuned viewing geometry or set of initial conditions. Regard-

ing viewing geometry: the libration of  $|\Delta\omega_{\text{sky}}|$  is similar to that of  $|\Delta\varpi_{\text{inv}}|$  for most observer orientations. Taking a single integration of HD 147018 for which  $|\Delta\varpi_{\text{inv}}|$  spends 60% of its time between  $75^\circ$  and  $135^\circ$  in the invariable plane, we viewed this system from the vantage points of 500 isotropically distributed observers. We find that 60% (80%) of observers measure  $75^\circ < |\Delta\omega_{\text{sky}}| < 135^\circ$  at least 50% (40%) of the time. Measurements from four example observers are given in the right column of Fig. 2. Regarding initial conditions: we numerically integrate different realizations of the five systems shown in Fig. 2, ignoring all observational constraints on  $\omega_{\text{sky}}$  and starting from various combinations of initial  $\{\varpi_{\text{inv},1}, \varpi_{\text{inv},2}, i_{\text{mut}}\}$ , with  $35^\circ < i_{\text{mut}} < 65^\circ$ . To simplify and speed up these calculations, we approximate the inner planet as a test particle and integrate the secular equations of motion (described further below). Among the many realizations thus constructed (three are shown in Fig. S6 along with accompanying surfaces of section), we find that it is not unusual for  $\Delta\varpi_{\text{inv}}$  (and by extension  $\Delta\omega_{\text{sky}}$ ) to linger near  $90^\circ/270^\circ$  — i.e., it is not uncommon for  $\Delta\varpi_{\text{inv}}$  to librate about  $180^\circ$  with a libration amplitude of  $90^\circ$ . Actually, depending on initial conditions,  $\Delta\varpi_{\text{inv}}$  can librate about either  $180^\circ$  or  $0^\circ$  with a variety of amplitudes, as well as circulate, and we discuss later why warm Jupiters may prefer a libration amplitude near  $90^\circ$ .

The apsidal libration observed here has been seen in other celestial mechanical contexts; it is qualitatively similar to the “artichoke-shaped” (37) libration exhibited by Saturn’s irregular satellites Narvi (38) and, for some initial conditions, Pasiphae (37,39). Both Narvi and Pasiphae orbit Saturn with inclinations of  $\sim 140^\circ$  with respect to the plane of Saturn’s orbit about the Sun. In the context of triple stellar systems, “beatlike” patterns with superposed short and long-timescale oscillations, similar to those observed in Fig. 2, were noticed in the modeled eccentricity variations of systems with  $i_{\text{mut}} \sim 40^\circ$ , and attributed to interference between the quadrupolar and octupolar potentials (40). The configurations of interest here do not lie near any border between circulation and libration; i.e.,  $\Delta\varpi_{\text{inv}}$  librates about  $180^\circ$  with an amplitude

of  $90^\circ$ , not  $180^\circ$ . In particular, the dynamics responsible for how  $|\Delta\varpi_{\text{inv}}|$  lingers near  $90^\circ$  is dissimilar from the “borderline” behavior of nearly coplanar systems in which  $|\Delta\varpi_{\text{inv}}|$  speeds through  $180^\circ$  but does not linger near  $90^\circ$  (41, 42).

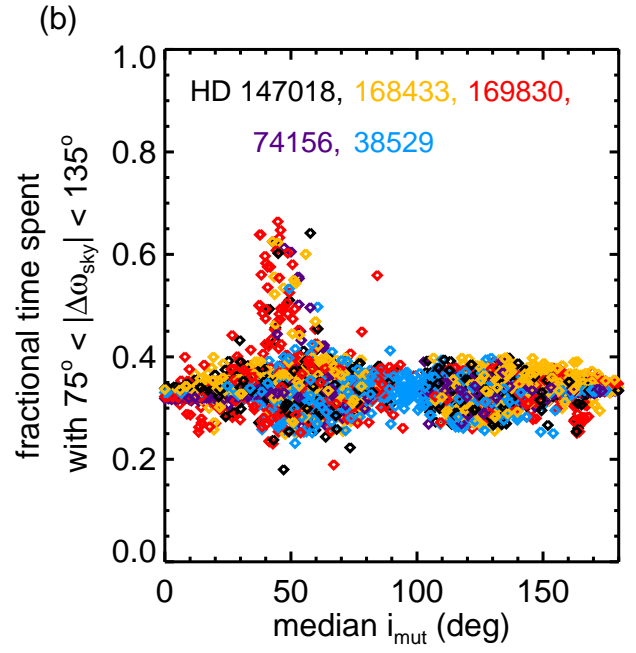
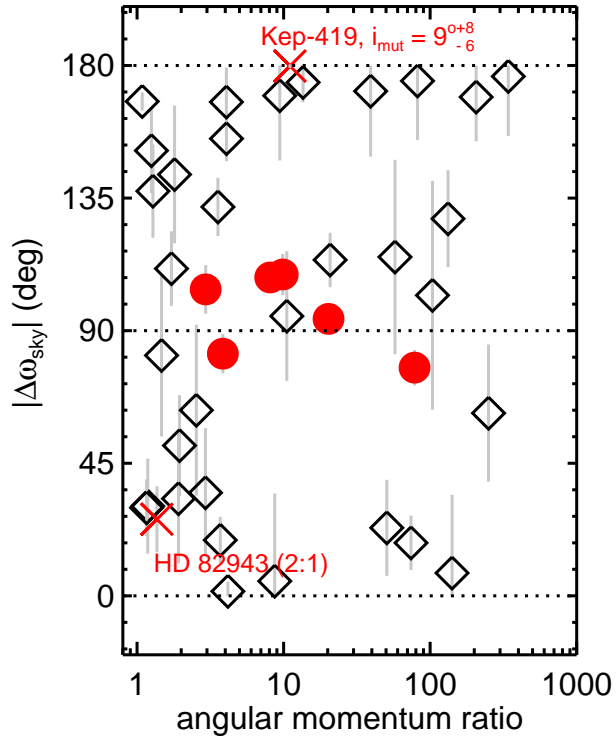
We can reproduce the observed libration of  $\Delta\varpi_{\text{inv}}$  by approximating a warm Jupiter as a test particle perturbed by an exterior body, and solving Lagrange’s equations of motion using a secular disturbing potential expanded to octupolar order (39), including general relativistic precession of both planets’ orbits (35). The octupolar potential plays an essential role in generating a precession rate  $d\Delta\varpi_{\text{inv}}/dt$  that cancels, on average, the precession rate induced by the quadrupolar potential; the net result is that  $\Delta\varpi_{\text{inv}}$  librates. Therefore the perturber must not only be near enough to dominate general relativistic precession (5, 23) but must also be eccentric: the strength of the octupolar potential is proportional to the perturber’s eccentricity. The importance of the octupolar potential has only recently been recognized in the exoplanet literature (6, 40). A popular application has been to flip an interior body from a prograde to retrograde orbit at large eccentricities (6, 43–47). A low mutual inclination, well below Kozai’s critical angle, is sufficient to spur such a flip if the inner planet’s eccentricity is high enough (46, 47). The regime explored here — which produces warm Jupiters with the observed clustering of  $|\Delta\omega_{\text{sky}}|$  near  $90^\circ$  — is complementary: both the inner and outer planets’ eccentricities are too modest for the octupolar potential to effect flips, and  $i_{\text{mut}}$  remains near  $40^\circ$ , a prograde configuration. Indeed we deduce that our six systems with warm Jupiters and close friends are prograde with  $i_{\text{mut}} \sim 40^\circ$  rather than retrograde with  $i_{\text{mut}} \sim 140^\circ$ , because in the latter case  $\omega_{\text{sky},1} + \omega_{\text{sky},2}$  would librate rather than  $\omega_{\text{sky},1} - \omega_{\text{sky},2}$  (39).

It is no coincidence that our six warm Jupiter systems are all characterized by mutual inclinations abutting Kozai’s minimum angle. In our regime in which the quadrupole potential still dominates and planetary eccentricities are low enough to avoid flips,  $39^\circ$  is the inclination that coincides with maximum eccentricity (minimum periaapse) and hence maximum tidal dis-

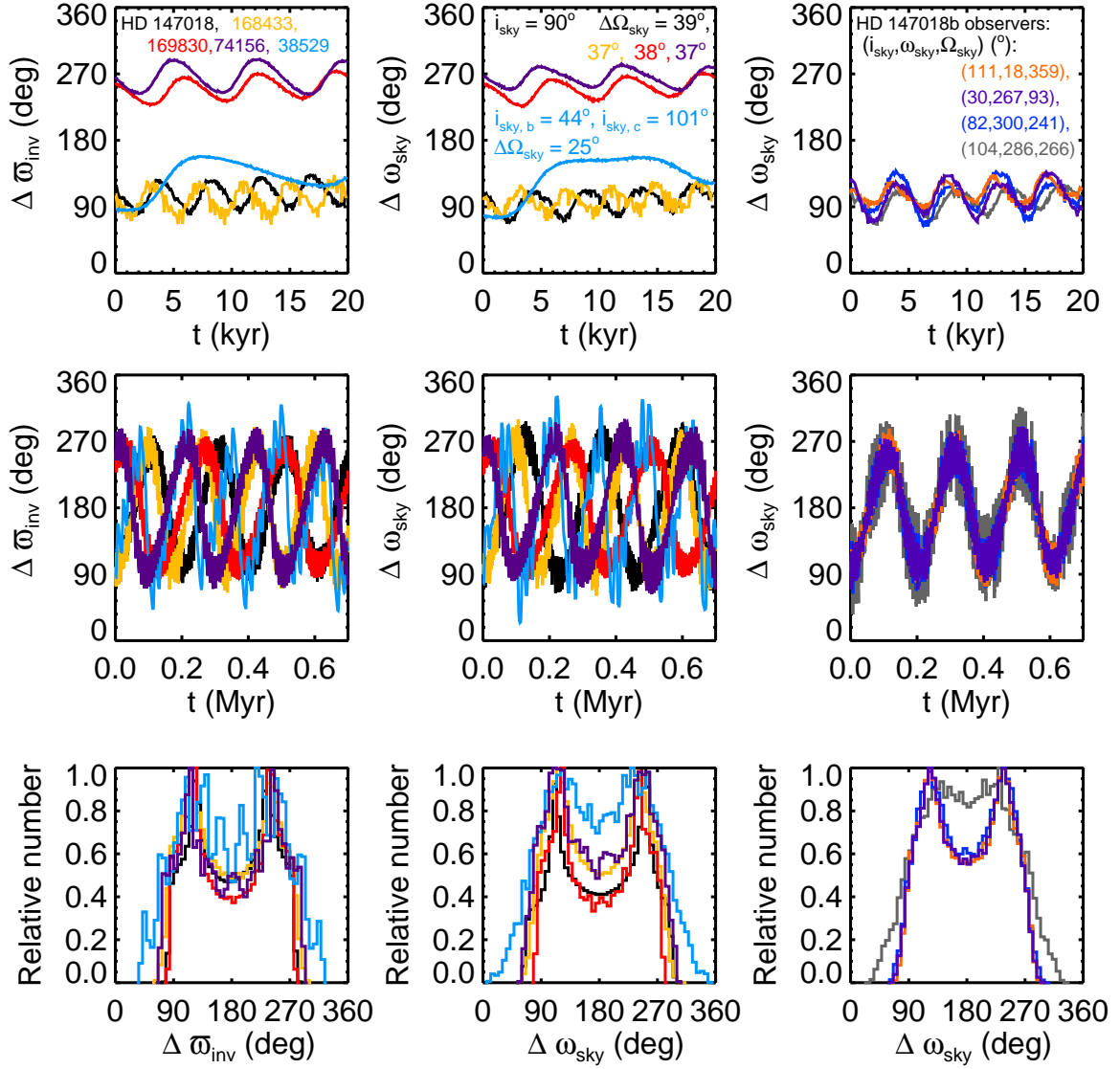
sipation. Orbital decay during this maximum-eccentricity, minimum-inclination phase of the Kozai cycle naturally leads to an abundance of tidally migrated warm Jupiters with  $i_{\text{mut}}$  near  $39\text{--}65^\circ$  (48). The octupolar potential is not strong enough for our systems to alter this feature of quadrupolar Kozai cycles (6, 48). At the same time, the reason why warm Jupiters have not completed their migration to become hot Jupiters is because of the special octupole-modified nature of their eccentricity variations. The usual (quadrupole) Kozai oscillations of eccentricity, which occur over the short nodal precession period, are modulated by an octupole-induced envelope (49) of much longer period following that of apsidal libration (Fig. 3; Figs. S1-S5). The envelope period is approximately  $(a_2/a_1)(1 - e_2^2)/e_2$  longer than the Kozai timescale (46). This long-period modulation prevents eccentricities from surging too often, and renders migration even slower than the “slow Kozai” migration described in (24). Such “super-slow” evolution is similar to the “step” migration seen at high  $i_{\text{mut}}$  (6), except without the transition from prograde to retrograde orbital motion and the accompanying rapid tidal circularization. In the gentle and intermittent migration considered here, warm Jupiters reach the small periapses characterizing hot Jupiters only at the peaks of their eccentricity envelopes. As a proof of concept, we perform an integration of the secular equations of motion including tidal friction (Fig. 4). The warm Jupiter undergoes super-slow tidal migration in which it librates apsidally and stalls in semi-major axis. A libration amplitude for  $\Delta\varpi_{\text{inv}}$  near  $90^\circ$  enables super-slow migration. If the libration amplitude were smaller, or if the apsidal separation were to circulate, then the envelope modulating the eccentricity would be less peaky, and the interior planet would spend more of its time near its maximum eccentricity. If the libration amplitude were larger, then not only would the apsidal separation be more prone to circulate given a small perturbation, but the system would also be more vulnerable to retrograde flips and concomitant eccentricity surges ( $e \rightarrow 1$ ). The upshot of all these scenarios in which  $\Delta\varpi_{\text{inv}}$  does not librate with an amplitude of  $90^\circ$  is that tidal migration, once begun, would rapidly complete and spawn a hot Jupiter (see

Fig. S7).

The class of warm Jupiters we have identified is similar to the predicted class of Kozai-oscillating warm Jupiters (23), except that here the octupolar field generated by the eccentricity of the exterior perturber plays a starring role in effecting the observed near-orthogonality of periaapse directions and in braking tidal migration. The mutual inclination of  $i_{\text{mut}} \sim 35\text{--}65^\circ$  we have inferred from the measured apsidal misalignment attests to how the Kozai mechanism, working between planets, has indeed shaped planetary systems. Although large inclinations between hot Jupiters' orbital planes and the equatorial planes of their host stars are well established, our finding provides evidence that pairs of more distant giant planets are themselves highly mutually inclined (although still prograde), in stark contrast to the flatness of solar system planets. The origin of such large inclinations is a mystery; planet-planet scattering (1) or secular chaos are possibilities (2).



**Fig. 1.** Apsidal misalignments between pairs of planets, and the large mutual inclinations implicated. Left (panel a): Sky-projected periaapse separations  $\Delta\omega_{\text{sky}}$  of planetary pairs, where  $-180^\circ < \Delta\omega_{\text{sky}} < 180^\circ$ . The sample includes all RV- and transit-discovered pairs with well-constrained (30) eccentricities and arguments of periaapse. No mass or semi-major axis cut is made on the black diamonds. The red circles (corresponding to systems shown also in Figs. 2–3 and S1–S5) and crosses (HD 82943, Kepler-419) represent warm Jupiters with one and only one known companion beyond 1 AU. All six of the red circles (51) lie close to  $|\Delta\omega_{\text{sky}}| = 90^\circ$ , i.e., their apsides are strongly misaligned. For calculation of the abscissa values, the orbital angular momentum is evaluated as  $m \sin i_{\text{sky}} \sqrt{a(1 - e^2)}$ . Right (panel b): Fraction of time that  $|\Delta\omega_{\text{sky}}|$  spends near  $90^\circ$ , as a function of median mutual inclination, for stable simulations of systems corresponding to five of the six red circles (the same five are shown in Fig. 2). HD 202206 is omitted; its architecture and apsidal behavior differ from those of the five (see Fig. S5). Each simulation is consistent with the observed orbital elements, but only those with  $i_{\text{mut}}$  near  $40^\circ$  spend extra time at  $|\Delta\omega_{\text{sky}}| \sim 90^\circ$ . The fractional time is evaluated for  $75^\circ < |\Delta\omega_{\text{sky}}| < 135^\circ$ ; this window is centered on  $105^\circ$  instead of  $90^\circ$  because of general relativistic precession.



**Fig. 2.** Sample time histories of apsidal misalignment for five planetary pairs of warm Jupiters and their outer companions. Initial conditions are taken from Table S1 with additional orbital angles indicated in the legend. For every history shown, the mutual inclination between the pair of planets varies within an interval that does not fall outside of  $35\text{--}65^\circ$ . Top: On short timescales, the apsidal separation lingers near  $90^\circ$  or  $270^\circ$ . Middle: Over longer timescales, the apsidal misalignment librates about  $180^\circ$  with an amplitude of  $90^\circ$ . Bottom: Relative oc-

currence of either the apsidal separation evaluated in the invariable plane ( $\Delta\varpi_{\text{inv}}$ ) or the sky-projected apsidal separation ( $\Delta\omega_{\text{sky}}$ ), in uniformly spaced bins, indicating that these angles spend excess time near  $90^\circ$  and  $270^\circ$ . Because of the lower oscillation frequencies characterizing HD 38529 and HD 74156, for these two systems we plot  $t/3$  as the abscissa in both top and middle rows. Unlike the systems shown here, HD 202206 is situated near the 5:1 resonance and its inner planet is almost certainly more massive than its outer planet (see Table S1); its dynamics is explored in Fig. S5.

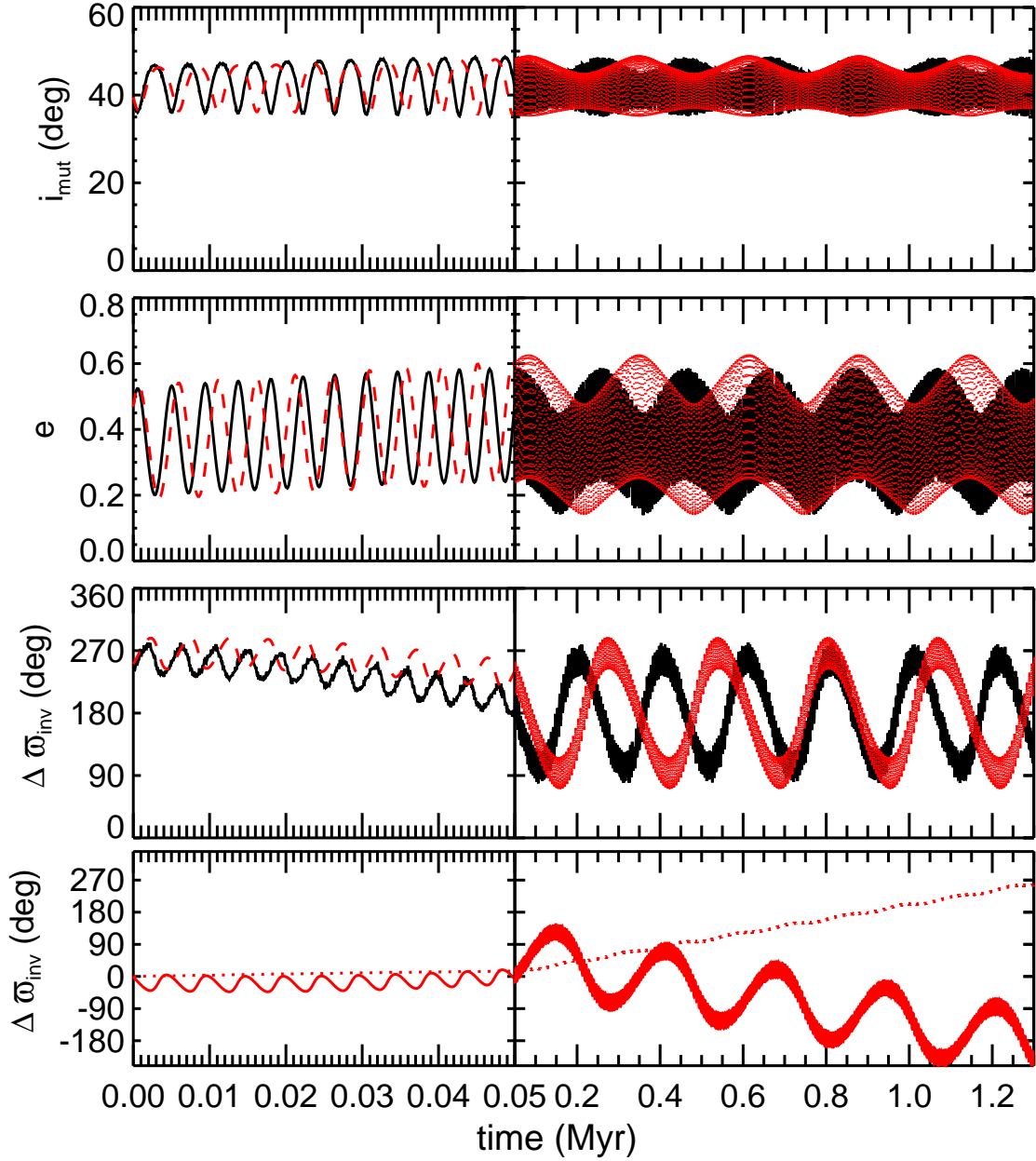


**Fig. 3.** Orbital evolution of HD 147018b, calculated using an  $N$ -body simulation and using a secular Hamiltonian expanded to octupolar order. Plotted are the time evolution of the mutual inclination (row 1), eccentricity of the inner warm Jupiter (row 2), apsidal separation (row 3), and near-canceling contributions to the apsidal separation from the quadrupolar and octupolar potentials (row 4). The simulation is performed in the invariable plane. Initial conditions are for

the HD 147018 system (Table S1) with  $i_{\text{sky}} = 90^\circ$  and  $\Delta\Omega_{\text{sky}} = 39^\circ$ , corresponding to  $i_{\text{mut}} = 39^\circ$  and to angles  $\{i_1 = 35.6^\circ, \omega_1 = 66.0^\circ, \Omega_1 = 0^\circ\}$  and  $\{i_2 = 3.4^\circ, \omega_2 = 136.9^\circ, \Omega_2 = 180^\circ\}$  in the invariable plane. All black curves in this figure are taken from the same `Mercury6`  $N$ -body integration underlying the black curves in the left column of Fig. 2. Red curves are for a test particle integrated using Lagrange’s equations of motion for the octupolar Hamiltonian (39). The bottom row was computed by separating the Hamiltonian into the quadrupolar terms (dotted line) and octupolar plus general-relativistic terms (solid line); by evaluating their respective contributions to  $\dot{\varpi}_1$  using Lagrange’s equations of motion; and by integrating  $\dot{\varpi}_1$ , setting the constant of integration to zero for simplicity. (The quantities  $e$  and  $i_{\text{mut}}$  were computed from the full Hamiltonian.) The sum of the dotted and solid curves in the bottom row equals the deviation of the red curve in the third row from its initial value. The secular behavior of the test particle reproduces qualitatively well that of the full  $N$ -body integration.

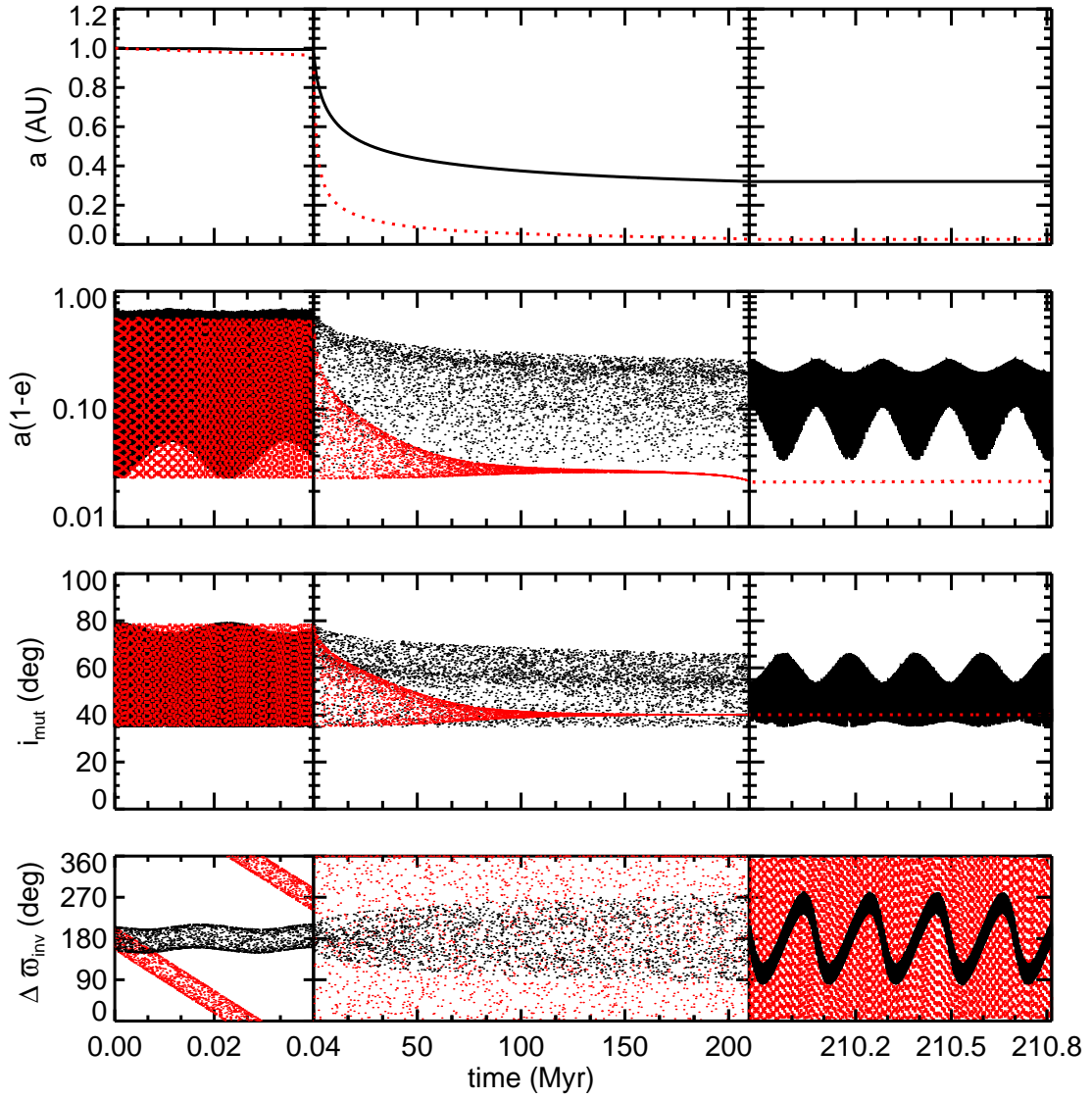


**Fig. 4.** Tidal migration under a secular potential expanded beyond quadrupolar order can produce a stalled warm Jupiter. Plotted are the time evolution of the inner planet’s semi-major axis, periastron distance, mutual inclination with the outer planet, and apsidal separation, integrated using the test particle Hamiltonian expanded to hexadecapolar order (39); practically identical results are obtained with the octupolar Hamiltonian. Overplotted are results from the Hamiltonian including only up to quadrupolar terms (red dashed) in which the inner planet

fails to stall and instead becomes a hot Jupiter. General relativistic precession is included for both planets (35). Tidal evolution is implemented using a constant tidal quality factor of  $10^5$ , a Love number of 0.26, and a planetary radius of 1 Jupiter radius (5). Tides raised on the star are not included because they are weak compared to tides raised on the planet at these semi-major axes. The tidal forcing frequency is set to  $\sqrt{\frac{G(M_\star+m_1)}{[a_1(1-e_1^2)]^3}}$  (22). The outer planet has  $a_2 = 1.923$  AU,  $e_2 = 0.133$ , and  $m_2 = 6.59M_{\text{Jupiter}}$ , matching HD 147018c, and initial  $\{i_2 = 0^\circ, \omega_2 = 17.2^\circ, \Omega_2 = 180^\circ\}$ . The inner planet (test particle) has initial  $a_1 = 1$  AU,  $e_1 = 0.9$ , and  $\{i_1 = 65^\circ, \omega_1 = 38.4^\circ, \Omega_1 = 0^\circ\}$ . With these choices, the eccentricity of the inner planet reaches a minimum of 0.33 at  $t = 220$  yr during the first Kozai cycle. The early tidal evolution, over the first  $\sim 20$  Myr, is subject to planet-planet scattering in a full  $N$ -body treatment; as such, the origin story portrayed in this figure is meant only to illustrate the concept of stalling, not to be definitive. This figure ends at  $\sim 200$  Myr but similar histories spanning a few Gyr are just as possible for different initial conditions or tidal efficiency factors.

## References and Notes

1. F. A. Rasio, E. B. Ford, *Science* **274**, 954 (1996).
2. Y. Wu, Y. Lithwick, *Astrophys. J.* **735**, 109 (2011).
3. Y. Kozai, *Astron. J.* **67**, 591 (1962).
4. M. L. Lidov, *Planetary and Space Science* **9**, 719 (1962).
5. Y. Wu, N. Murray, *Astrophys. J.* **589**, 605 (2003).
6. S. Naoz, W. M. Farr, Y. Lithwick, F. A. Rasio, J. Teysandier, *Nature* **473**, 187 (2011).
7. G. Takeda, F. A. Rasio, *Astrophys. J.* **627**, 1001 (2005).
8. M. Jurić, S. Tremaine, *Astrophys. J.* **686**, 603 (2008).
9. D. Fabrycky, S. Tremaine, *Astrophys. J.* **669**, 1298 (2007).
10. Y. Wu, N. W. Murray, J. M. Ramsahai, *Astrophys. J.* **670**, 820 (2007).
11. S. Chatterjee, E. B. Ford, S. Matsumura, F. A. Rasio, *Astrophys. J.* **686**, 580 (2008).
12. M. Nagasawa, S. Ida, *Astrophys. J.* **742**, 72 (2011).
13. T. D. Morton, J. A. Johnson, *Astrophys. J.* **738**, 170 (2011).
14. S. Naoz, W. M. Farr, F. A. Rasio, *Astrophys. J. L.* **754**, L36 (2012).
15. E. J. Rivera, *et al.*, *Astrophys. J.* **719**, 890 (2010).
16. R. Sanchis-Ojeda, *et al.*, *Nature* **487**, 449 (2012).
17. M. H. Lee, S. J. Peale, *Astrophys. J.* **567**, 596 (2002).

18. B. E. McArthur, *et al.*, *Astrophys. J.* **715**, 1203 (2010).
19. R. I. Dawson, *et al.*, *Astrophys. J.* **791**, 89 (2014).
20. A. Cumming, *et al.*, *Pub. Astron. Soc. Pac.* **120**, 531 (2008).
21. C. Petrovich, S. Tremaine, R. Rafikov, *Astrophys. J.* **786**, 101 (2014).
22. A. Socrates, B. Katz, S. Dong, *ArXiv e-prints* (2012), arXiv:1209.5724.
23. S. Dong, B. Katz, A. Socrates, *Astrophys. J. L.* **781**, L5 (2014).
24. C. Petrovich, *ArXiv e-prints* (2014), arXiv:1405.0280.
25. H. A. Knutson, *et al.*, *Astrophys. J.* **785**, 126 (2014).
26. R. I. Dawson, R. A. Murray-Clay, *Astrophys. J. L.* **767**, L24 (2013).
27. E. I. Chiang, S. Tabachnik, S. Tremaine, *Astron. J.* **122**, 1607 (2001).
28. T. A. Michtchenko, R. Malhotra, *Icarus* **168**, 237 (2004).
29. Queried from the Exoplanet Orbit Database (EOD) at exoplanets.org (50) on April 8, 2014.
30. Eccentricity detected at two-sigma, and  $\Delta\omega_{\text{sky}}$  detected with an uncertainty of  $< \pm 40^\circ$ .
31. We select for eccentric warm Jupiters with only one known companion, as additional companions can disrupt Kozai oscillations. Our selection criterion thus excludes planetary pairs that are members of the 55 Cnc, epsilon Andromeda, mu Arae, HIP 14810, Kepler-9, and Kepler-30 systems. Moreover, each of these systems also has a close-in ( $a < 0.1$  AU) planet that would be disrupted if the warm Jupiter were to attain periastron distances small enough for tidal circularization.
32. X. Tan, *et al.*, *Astrophys. J.* **777**, 101 (2013).

33. For HD 202206c, modification of the semi-major axis from the best-fit value was required to avoid libration in the 5:1 resonance. See Supplementary Materials for details.
34. J. E. Chambers, *Mon. Not. R. Astron. Soc.* **304**, 793 (1999).
35. D. C. Fabrycky, in *Exoplanets*, S. Seager, Ed. (University of Arizona Press, Tuscon, 2011), pp. 217–238.
36. D. Veras, E. B. Ford, *Astrophys. J.* **715**, 803 (2010).
37. A. L. Whipple, P. J. Shelus, *Icarus* **101**, 265 (1993).
38. J. Correa Otto, A. M. Leiva, C. A. Giuppone, C. Beaugé, *Mon. Not. R. Astron. Soc.* **402**, 1959 (2010).
39. T. Yokoyama, M. T. Santos, G. Cardin, O. C. Winter, *Astron. Astrophys.* **401**, 763 (2003).
40. E. B. Ford, B. Kozinsky, F. A. Rasio, *Astrophys. J.* **535**, 385 (2000).
41. R. Barnes, R. Greenberg, *Astrophys. J. L.* **659**, L53 (2007).
42. E. B. Ford, *IAU Symposium 249*, Y.-S. Sun, S. Ferraz-Mello, J.-L. Zhou, eds. (2008), vol. 249 of *IAU Symposium*.
43. B. Katz, S. Dong, R. Malhotra, *Physical Review Letters* **107**, 181101 (2011).
44. Y. Lithwick, S. Naoz, *Astrophys. J.* **742**, 94 (2011).
45. S. Naoz, W. M. Farr, Y. Lithwick, F. A. Rasio, J. Teyssandier, *Mon. Not. R. Astron. Soc.* **431**, 2155 (2013).
46. G. Li, S. Naoz, B. Kocsis, A. Loeb, *Astrophys. J.* **785**, 116 (2014).
47. G. Li, S. Naoz, M. Holman, A. Loeb, *Astrophys. J.* **791**, 86 (2014).

48. L. G. Kiseleva, P. P. Eggleton, S. Mikkola, *Mon. Not. R. Astron. Soc.* **300**, 292 (1998).
49. The eccentricity of HD 202206b does not have such an envelope (Fig. S5), which may be due to its proximity to the 5:1 mean-motion resonance and the large relative mass of the inner planet.
50. J. T. Wright, *et al.*, *Pub. Astron. Soc. Pac.* **123**, 412 (2011).
51. Among the black diamonds, the planetary pairs with  $|\Delta\omega_{\text{sky}}|$  near  $90^\circ$  and large angular momentum ratios include giant planets in a five-planet system (55 Cnc), a pair of hot super-Earths (GJ 163), and a cold Jupiter partnered with a hot Neptune (HD 125612); it is unclear whether their orthogonal eccentricity vectors also signify large mutual inclinations. The transiting pair Kepler-30 c and d, which are near a 2:1 resonance, have  $|\Delta\omega_{\text{sky}}| = 114^\circ$ , an angular momentum ratio of 21, and a low mutual inclination (16).
52. J. Couetdic, J. Laskar, A. C. M. Correia, M. Mayor, S. Udry, *Astron. Astrophys.* **519**, A10 (2010).
53. R. V. Baluev, C. Beaugé, *Mon. Not. R. Astron. Soc.* **439**, 673 (2014).
54. D. Ségransan, *et al.*, *Astron. Astrophys.* **511**, A45 (2010).
55. J. T. Wright, *et al.*, *Astrophys. J.* **693**, 1084 (2009).
56. We use the corrected elements reported by the EOD.
57. G. Pilyavsky, *et al.*, *Astrophys. J.* **743**, 162 (2011).
58. S. Meschiari, *et al.*, *Astrophys. J.* **727**, 117 (2011).
59. M. Mayor, *et al.*, *Astron. Astrophys.* **415**, 391 (2004).

60. Original solution listed in EOD.
61. A. C. M. Correia, *et al.*, *Astron. Astrophys.* **440**, 751 (2005).
62. Best-fit  $N$ -body solution (52), for which we have adjusted  $a_2$  to obtain the results shown in Fig. S5.
63. In an independent analysis of the data, evidence was found for a third planet, not listed here (53).

**Acknowledgements:** We gratefully acknowledge support from the Miller Institute for Basic Research in Science, the University of California (UC) Berkeley’s Center for Integrative Planetary Science, the National Science Foundation, and the National Aeronautics and Space Administration. This research has made use of the Exoplanet Orbit Database at [exoplanets.org](http://exoplanets.org). This research employed the SAVIO computational cluster provided by the Berkeley Research Computing program, which is supported by UC Berkeley’s Chancellor, Vice Chancellor for Research, and Chief Information Officer. We thank four anonymous referees for constructive feedback and Daniel Fabrycky and John Johnson for helpful comments.

## Supplementary Materials

Figures S1–S7

Table S1

References (52–63)

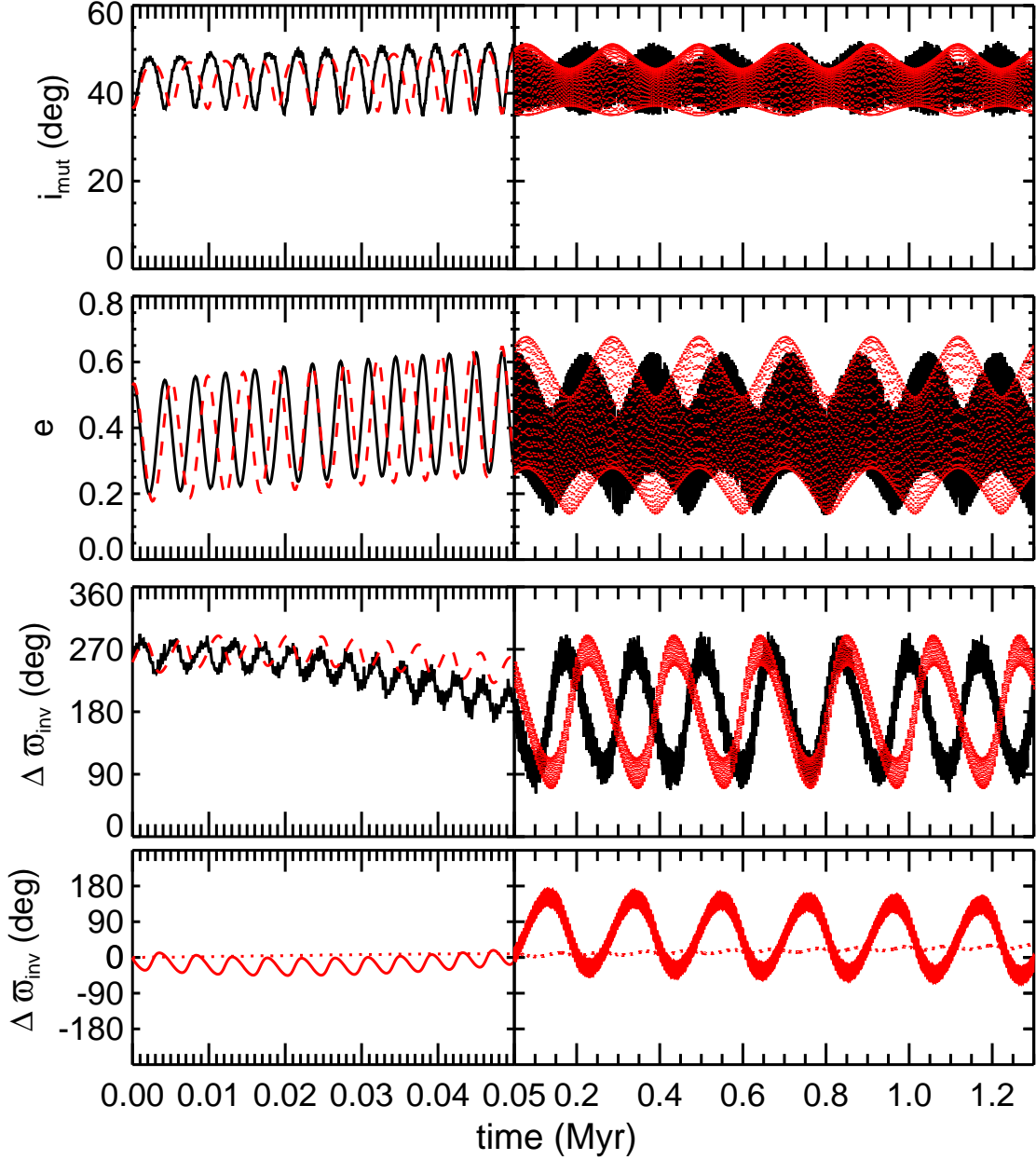


**Fig. S1.**

Orbital evolution of HD 168433b, calculated using an  $N$ -body simulation and using a secular Hamiltonian expanded to octupolar order. Plotted are the time evolution of the mutual inclination (row 1), eccentricity of the inner warm Jupiter (row 2), apical separation (row 3), and near-canceling contributions to the apical separation from the quadrupolar and octupolar potentials (row 4). The simulations were performed in the invariable plane. Initial conditions were for the HD 168433 system (Table S1) with  $i_{\text{sky}} = 90^\circ$  and  $\Delta\Omega_{\text{sky}} = 37^\circ$ , corresponding to  $i_{\text{mut}} = 37^\circ$  and to angles  $\{i_1 = 33.1^\circ, \omega_1 = 263.0^\circ, \Omega_1 = 0^\circ\}$  and  $\{i_2 = 3.9^\circ, \omega_2 = 334.3^\circ, \Omega_2 = 180^\circ\}$  in

the invariable plane. All black curves in this figure are taken from the same Mercury6  $N$ -body integration underlying the yellow curves in the left column of Fig. 2. Red curves are for a test particle integrated using Lagrange's equations of motion for the octupolar Hamiltonian (39). The bottom row was computed by separating the Hamiltonian into the quadrupolar terms (dotted line) and octupolar plus general-relativistic terms (solid line); by evaluating their respective contributions to  $\dot{\varpi}_1$  using Lagrange's equations of motion; and by integrating  $\dot{\varpi}_1$ , setting the constant of integration to zero for simplicity. (The quantities  $e$  and  $i_{\text{mut}}$  were computed from the full Hamiltonian.) The sum of the dotted and solid curves in the bottom row equals the deviation of the red curve in the third row from its initial value. The secular behavior of the test particle reproduces qualitatively well that of the full  $N$ -body integration.

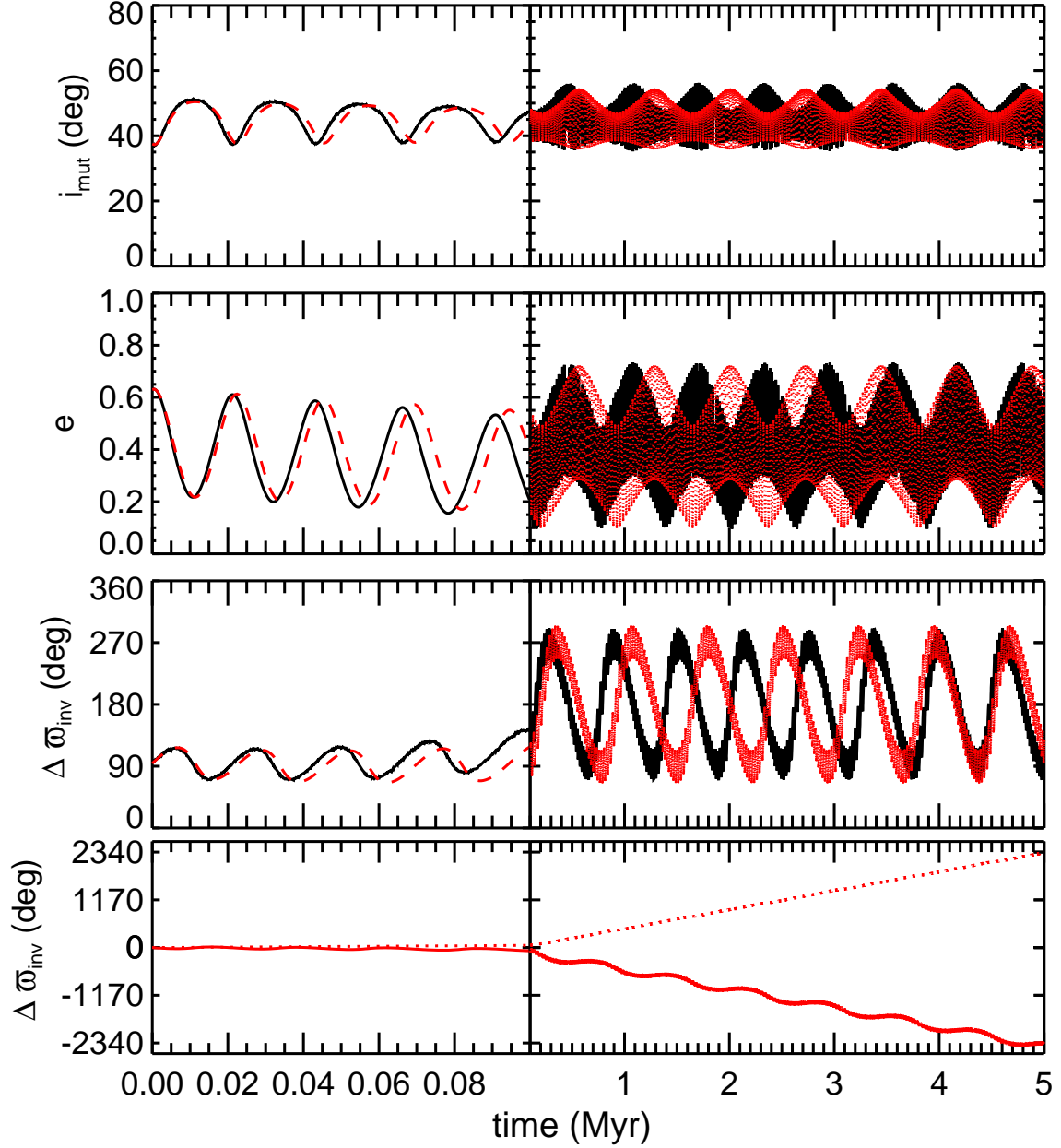


**Fig. S2.**

Orbital evolution of HD 74156b, calculated using an  $N$ -body simulation and using a secular Hamiltonian expanded to octupolar order. Plotted are the time evolution of the mutual inclination (row 1), eccentricity of the inner warm Jupiter (row 2), apsidal separation (row 3), and near-canceling contributions to the apsidal separation from the quadrupolar and octupolar potentials (row 4). The simulation was performed in the invariable plane. Initial conditions were for the HD 74156 system (Table S1) with  $i_{\text{sky}} = 90^\circ$  and  $\Delta\Omega_{\text{sky}} = 37^\circ$ , corresponding to  $i_{\text{mut}} = 37^\circ$  and to angles  $\{i_1 = 35.4^\circ, \omega_1 = 84.0^\circ, \Omega_1 = 0^\circ\}$  and  $\{i_2 = 1.6^\circ, \omega_2 = 358.1^\circ, \Omega_2 = 180^\circ\}$

in the invariable plane. All black curves in this figure are taken from the same `Mercury6`  $N$ -body integration underlying the purple curves in the left column of Fig. 2. Red curves are for a test particle integrated using Lagrange's equations of motion for the octupolar Hamiltonian (39). The bottom row was computed by separating the Hamiltonian into the quadrupolar terms (dotted line) and octupolar plus general-relativistic terms (solid line); by evaluating their respective contributions to  $\dot{\varpi}_1$  using Lagrange's equations of motion; and by integrating  $\dot{\varpi}_1$ , setting the constant of integration to zero for simplicity. (The quantities  $e$  and  $i_{\text{mut}}$  were computed from the full Hamiltonian.) The sum of the dotted and solid curves in the bottom row equals the deviation of the red curve in the third row from its initial value. The secular behavior of the test particle reproduces qualitatively well that of the full  $N$ -body integration.

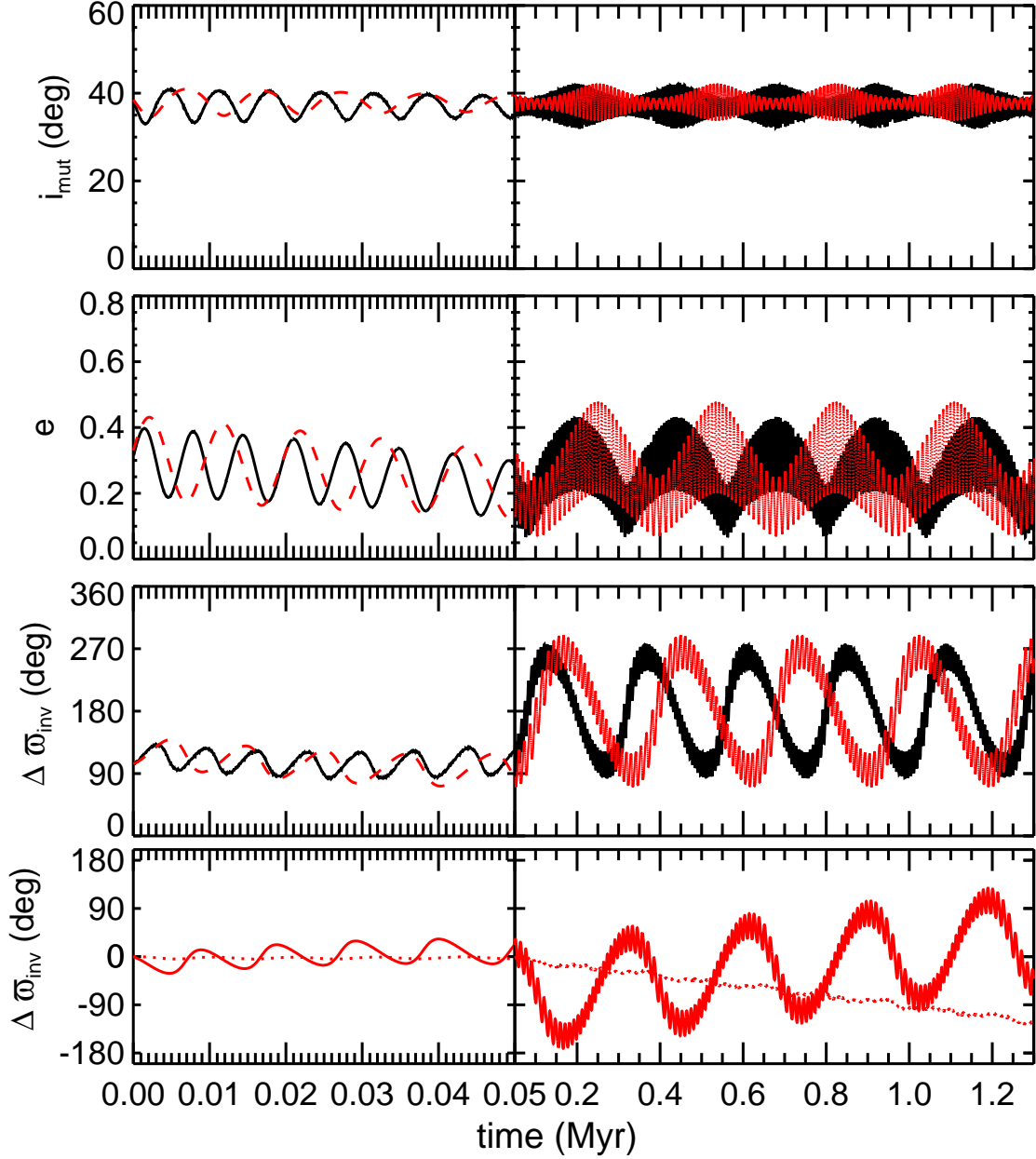


**Fig. S3.**

Orbital evolution of HD 169830b, calculated using an  $N$ -body simulation and using a secular Hamiltonian expanded to octupolar order. Plotted are the time evolution of the mutual inclination (row 1), eccentricity of the inner warm Jupiter (row 2), apical separation (row 3), and near-canceling contributions to the apical separation from the quadrupolar and octupolar potentials (row 4). The simulation was performed in the invariable plane. Initial conditions were for the HD 169830 system (Table S1) with  $i_{\text{sky}} = 90^\circ$  and  $\Delta\Omega_{\text{sky}} = 38^\circ$ , corresponding to  $i_{\text{mut}} = 38^\circ$  and to angles  $\{i_1 = 28.6^\circ, \omega_1 = 238.0^\circ, \Omega_1 = 0^\circ\}$  and  $\{i_2 = 9.4^\circ, \omega_2 = 162.0^\circ, \Omega_2 = 180^\circ\}$

in the invariable plane. All black curves in this figure are taken from the same `Mercury6`  $N$ -body integration underlying the red curves in the left column of Fig. 2. Red curves here are for a test particle integrated using Lagrange’s equations of motion for the octupolar Hamiltonian (39). The bottom row was computed by separating the Hamiltonian into the quadrupolar terms (dotted line) and octupolar plus general-relativistic terms (solid line); by evaluating their respective contributions to  $\dot{\varpi}_1$  using Lagrange’s equations of motion; and by integrating  $\dot{\varpi}_1$ , setting the constant of integration to zero for simplicity. (The quantities  $e$  and  $i_{\text{mut}}$  were computed from the full Hamiltonian.) The sum of the dotted and solid curves in the bottom row equals the deviation of the red curve in the third row from its initial value. The secular behavior of the test particle reproduces qualitatively well that of the full  $N$ -body integration.

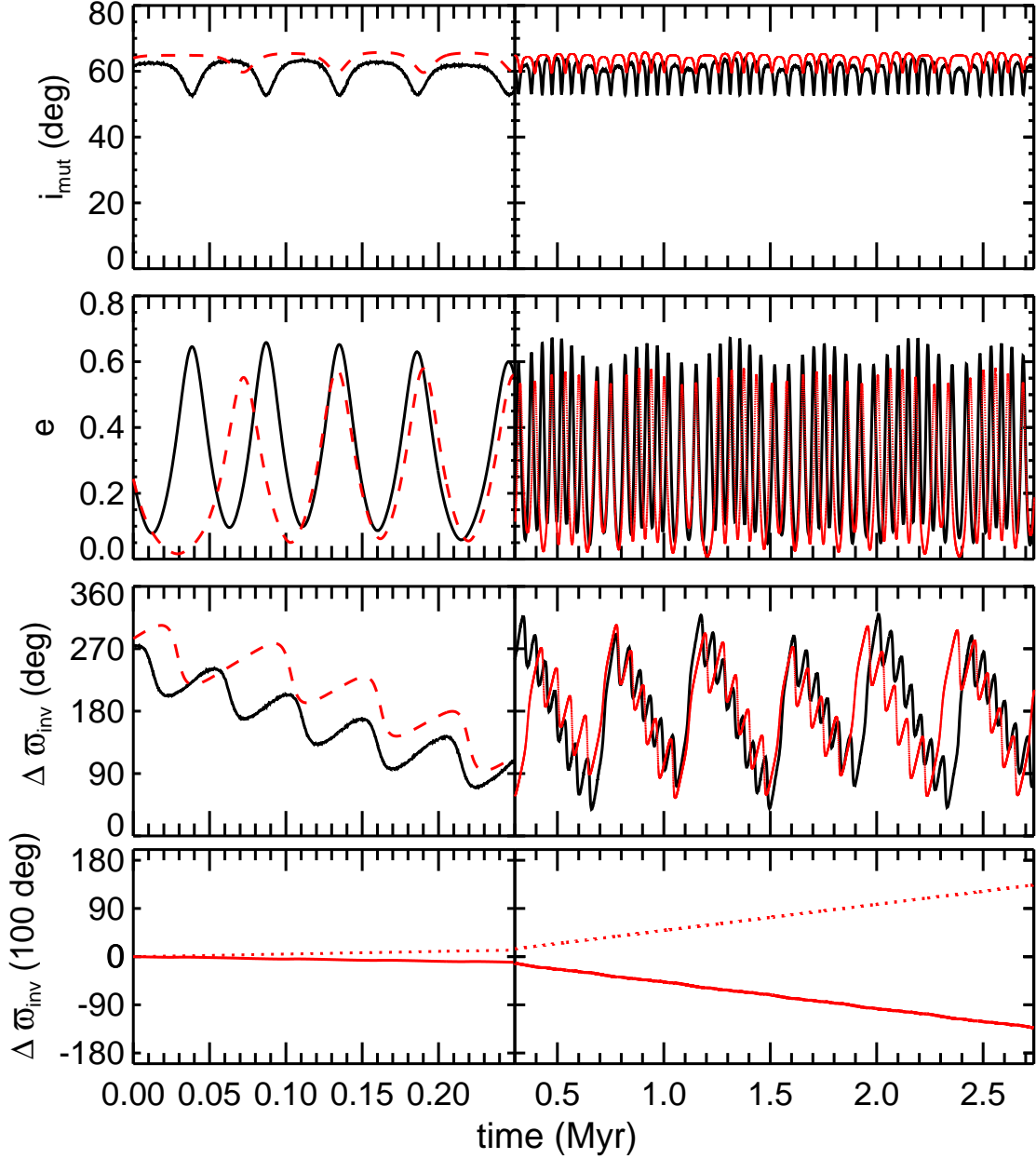


**Fig. S4.**

Orbital evolution of HD 38529b, calculated using an  $N$ -body simulation and using a secular Hamiltonian expanded to octupolar order. Plotted are the time evolution of the mutual inclination (row 1), eccentricity of the inner warm Jupiter (row 2), apical separation (row 3), and near-canceling contributions to the apical separation from the quadrupolar and octupolar potentials (row 4). Initial conditions were for the HD 38529 system (Table S1) with  $i_{\text{sky},1} = 43.7^\circ$ ,  $i_{\text{sky},2} = 100.8^\circ$ ,  $\Delta\Omega_{\text{sky}} = 25^\circ$ , corresponding to  $i_{\text{mut}} = 61.4^\circ$  and to angles  $\{i_1 = 60.5^\circ, \omega_1 = 303.6^\circ, \Omega_1 = 0^\circ\}$  and  $\{i_2 = 0.9^\circ, \omega_2 = 37.9^\circ, \Omega_2 = 180^\circ\}$  in the invariable

plane. All black curves in this figure are taken from the same `Mercury6`  $N$ -body integration underlying the blue curves in the left column of Fig. 2. Red curves are for a test particle integrated using Lagrange’s equations of motion for the octupolar Hamiltonian (39). The bottom row was computed by separating the Hamiltonian into the quadrupolar terms (dotted line) and octupolar plus general-relativistic terms (solid line); by evaluating their respective contributions to  $\dot{\varpi}_1$  using Lagrange’s equations of motion; and by integrating  $\dot{\varpi}_1$ , setting the constant of integration to zero for simplicity. (The quantities  $e$  and  $i_{\text{mut}}$  were computed from the full Hamiltonian.) The sum of the dotted and solid curves in the bottom row equals the deviation of the red curve in the third row from its initial value. The secular behavior of the test particle reproduces qualitatively well that of the full  $N$ -body integration.

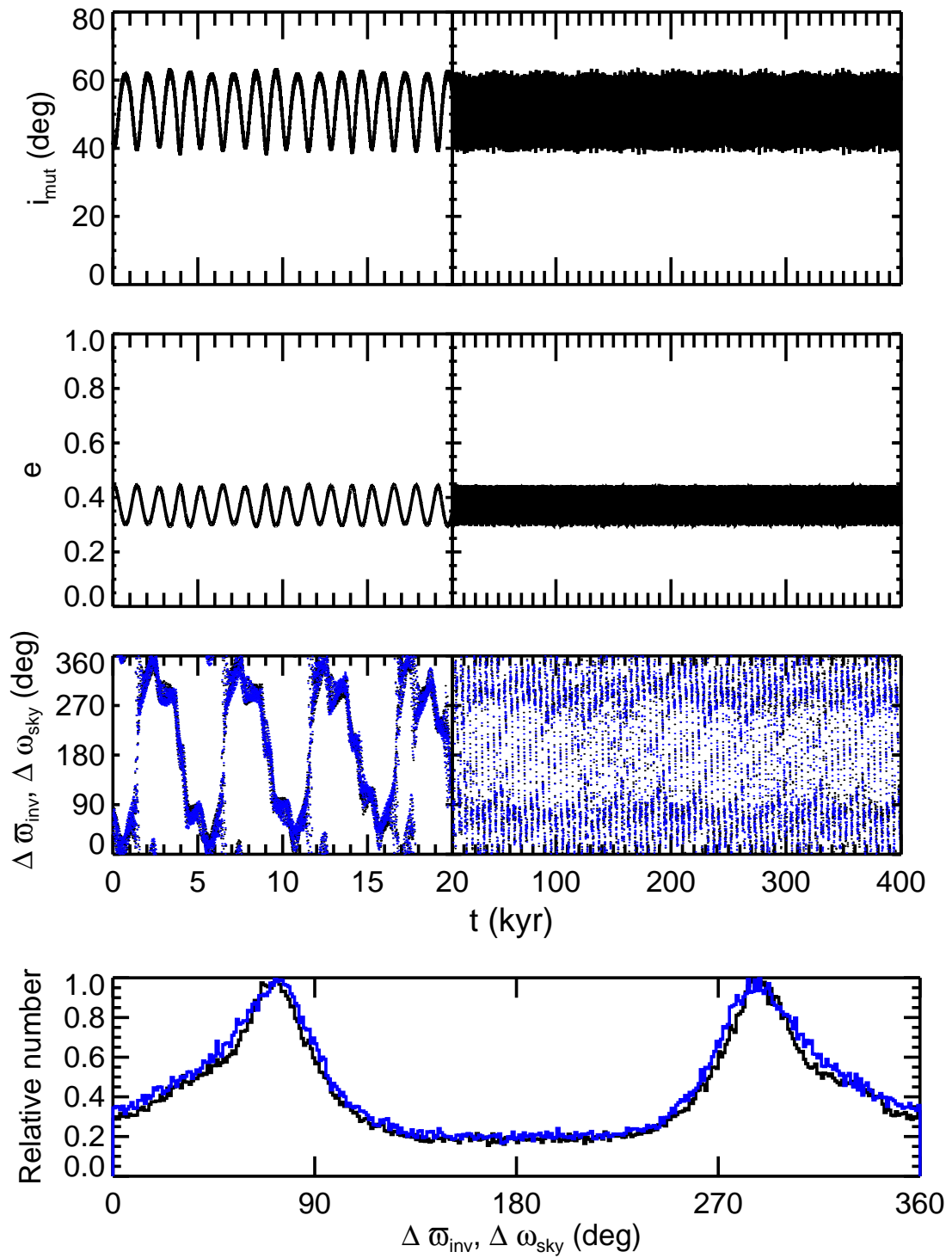


**Fig. S5.** Orbital evolution of HD 22206, calculated using an  $N$ -body simulation performed in the in-

variable plane. The projection  $\Delta\omega_{\text{sky}}$  is overplotted in blue. Initial conditions were taken from the reported best-fit  $N$ -body solution (52), with the semi-major axis of the outer planet decreased (away from the 5:1 resonance) to the two-sigma lower limit from the observations,  $a_2 = 2.43$  AU (see the second entry for HD 202206 in Table S1). The initial orbital orientation angles were  $i_{\text{sky}} = 90^\circ$  and  $\Delta\Omega_{\text{sky}} = 41^\circ$  in the sky plane, corresponding to  $i_{\text{mut}} = 41^\circ$  and to  $\{i_1 = 7.9^\circ, \omega_1 = 71.9^\circ, \Omega_1 = 311^\circ\}$  and  $\{i_2 = 33.1^\circ, \omega_2 = 195.5^\circ, \Omega_2 = 131^\circ\}$  in the invariable plane. In contrast to the other five systems shown in Figs. 2–3 and Figs. S1–S4, the HD 202206 system cannot be modeled in the test particle approximation using a purely secular Hamiltonian because of the system’s proximity to the 5:1 resonance and the large relative mass of the inner planet ( $\min m_1 = 16.59M_{\text{Jupiter}}$ ,  $\min m_2 = 2.179M_{\text{Jupiter}}$ ). Nevertheless, as illustrated in the bottom panel, the system still shows a tendency to be found with its apses nearly orthogonally misaligned.

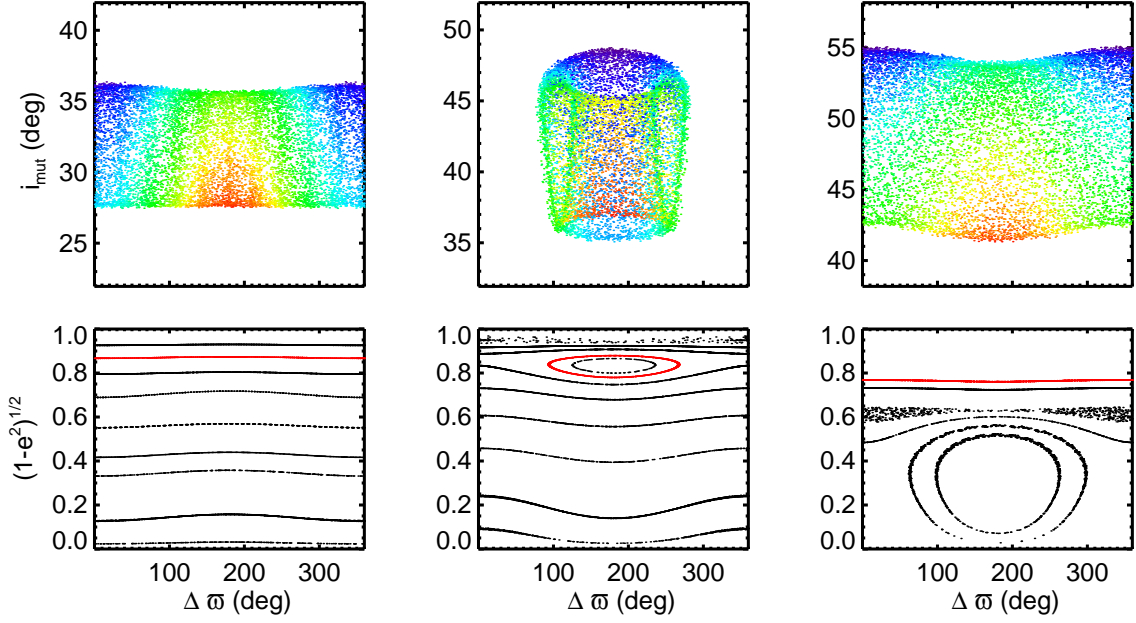


**Fig. S6.**

Trajectories of HD 147018b illustrating the lingering of  $\Delta\varpi_{\text{inv}}$  near  $90^\circ/270^\circ$  and libration of  $\Delta\varpi_{\text{inv}}$  about  $180^\circ$  for  $i_{\text{mut}} \sim 40^\circ$ . Top row: Full trajectories from Mercury6 integrations performed in the invariable plane. The colors are contours of the inner planet's  $z$ -component of angular momentum. Each column represents an integration that starts from a different mutual inclination:  $29^\circ$ ,  $39^\circ$ ,  $49^\circ$  from left to right (equivalently,  $i_1 = 26.4^\circ$ ,  $35.6^\circ$ ,  $44.9^\circ$ , respectively, in the invariable plane). All other initial conditions matched those in Fig. 3; the second column is the same integration as shown in Fig. 3, and depicts the lingering of  $\Delta\varpi_{\text{inv}}$  near  $90^\circ/270^\circ$  as two hollowed-out green lobes. We note that each column represents an individual trajectory; these are not Hamiltonian contour plots. Bottom row: Surfaces of section for the secular test-particle Hamiltonian (39), expanded to octupolar order and including general relativistic precession for the inner planet. Each panel corresponds to a value for the Hamiltonian equal to that in the trajectory in the row above, which is plotted in red; trajectories of equal Hamiltonian value but different initial conditions are plotted in black. Points are plotted whenever  $\omega_1 = 90^\circ$ . Only the middle panel features the sought-after libration of  $\Delta\varpi$  about  $180^\circ$  at the observed moderate  $e_1$ . The trajectories shown are selected by fixing  $\varpi_2 = 316.865^\circ$ .

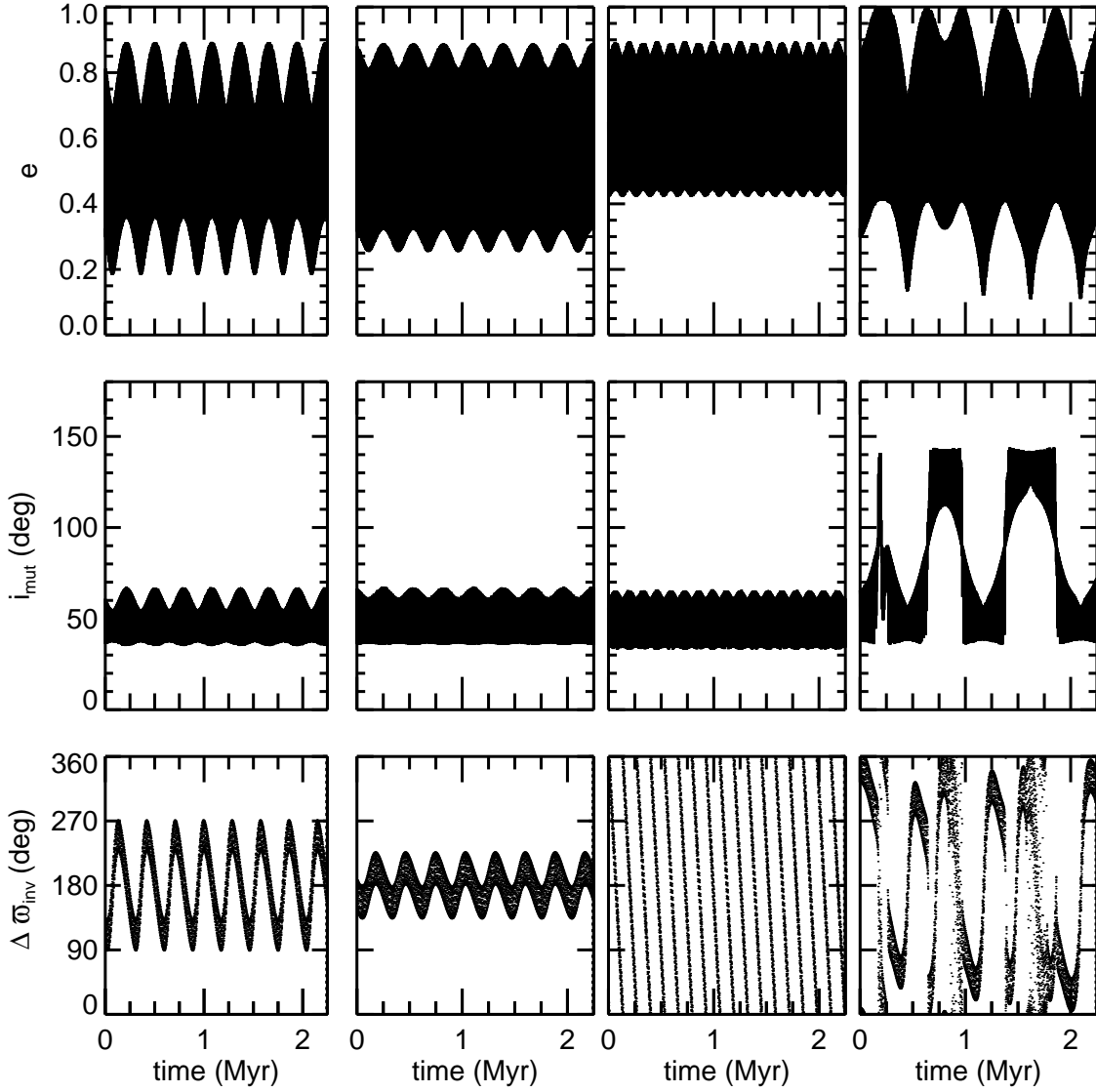


**Fig. S7.**

Four integrations showing the range of behaviors possible for  $\Delta\varpi_{\text{inv}}$ ,  $e$ , and  $i_{\text{mut}}$ . We used the test particle Hamiltonian expanded to hexadecapolar order (39); virtually identical results are obtained to octupolar order. Initial conditions of column 1 were taken from  $t = 150$  Myr of Fig. 4:  $\{a_1 = 0.34 \text{ AU}, \Omega_1 = 160.3^\circ, a_2 = 1.923 \text{ AU}, e_2 = 0.133, i_2 = 0^\circ, \Omega_2 = 340.3^\circ\}$ . Initial conditions for the other columns are the same except with  $\{e_1 = 0.325, i_1 = 60.5^\circ, \omega_1 = 162.6^\circ, \varpi_2 = 90.1^\circ\}$  (column 1);  $\{e_1 = 0.35, i_1 = 66^\circ, \omega_1 = 162.6^\circ, \varpi_2 = 340.1^\circ\}$  (column 2);  $\{e_1 = 0.65, i_1 = 55^\circ, \omega_1 = 143.4^\circ, \varpi_2 = 320.9^\circ\}$  (column 3); and  $\{e_1 = 0.325, i_1 = 65^\circ, \omega_1 = 162.6^\circ, \varpi_2 = 322.9^\circ\}$  (column 4). The angle  $\varpi = \Omega - \omega$  when  $i > 90^\circ$  (37). Column 1:  $\Delta\varpi_{\text{inv}}$  lingers near  $90^\circ/270^\circ$  and the eccentricity has a strongly modulated envelope; the planet spends little time near its minimum periape (maximum  $e$ ). Column 2: A smaller

libration amplitude for  $\Delta\varpi_{\text{inv}}$  is accompanied by a less peaky modulation of eccentricity; the planet spends more time near minimum periapse as compared to Column 1. Column 3:  $\Delta\varpi_{\text{inv}}$  circulates and eccentricity spends more time near its maximum value than in Column 1. Column 4: For a large libration amplitude for  $\Delta\varpi_{\text{inv}}$  and just slightly larger initial  $i_{\text{mut}}$ , the planet is subject to inclination flips and eccentricity surges. When combined with tidal friction, the behavior in Columns 2–4 can lead to rapid tidal migration and the formation of hot Jupiters, whereas the behavior in Column 1 can produce stalled warm Jupiters.

Table 1: Observed orbital elements of seven RV-detected systems (50) and one transit-detected system (19) comprising warm ( $0.1 < a$  (AU)  $< 1$ ) Jupiters and their close friends ( $a > 1$  AU). Only systems with a single pair of planets and securely measured eccentricities and  $\omega_{\text{sky}}$  are listed (30, 31).

System	$a_1$	$a_2$	$e_1$	$e_2$	$m_1$	$m_2$	$\omega_{\text{sky},1}$	$\omega_{\text{sky},2}$	$ \Delta\omega_{\text{sky}} $	Ref.
	(AU)	(AU)			$\sin i_{\text{sky},1}$	$\sin i_{\text{sky},2}$	( $\circ$ )	( $\circ$ )	( $\circ$ )	
					( $M_{\text{Jupiter}}$ )	( $M_{\text{Jupiter}}$ )				
HD										
147018	0.239	1.92	0.469	0.133	2.127	6.59	336.0	226.9	109.1	(54)
38529	0.127	3.60	0.244	0.355	0.803	12.26	95.4	17.9	77.5	(55)
168443 (56)	0.294	2.85	0.529	0.211	7.70	17.39	172.9	64.87	108.1	(57)
74156	0.292	3.90	0.630	0.380	1.773	8.25	174.0	268.0	266.0	(58)
169830	0.813	3.60	0.310	0.330	2.89	4.06	148.0	252.0	104.0	(59)
202206 (60)	0.812	2.49	0.435	0.267	16.82	2.33	161.2	79.0	92.2	(61)
202206 (62)	0.805	2.43	0.431	0.104	16.59	2.179	161.9	105.6	56.3	(52)
82943 (63)	0.742	1.19	0.425	0.203	1.59	1.589	133	107	26	(32)
Kepler-419	0.370	1.68	0.833	0.184	2.5	7.3	95.2	275.3	179.8	(19)